

Research Article

Open Access



Bandgap engineering of $\text{Zn}_{1-x}\text{Cd}_x\text{S}$ for glycerol photo(electro)reforming into glyceric acid with hydrogen coproduction

Xinti Yu^{1,2,#}, Daichen Liu^{1,#}, Ce Fu², Bokun Zhu², Xue Yong³, Jinguang Hu^{1,*}, Heng Zhao^{2,*}, Zhangxing Chen^{2,4,*}

¹Department of Chemical and Petroleum Engineering, University of Calgary, Calgary, Alberta T2N 1N4, Canada.

²College of Engineering, Eastern Institute of Technology, Ningbo 315200, Zhejiang, China.

³Department of Electrical Engineering and Electronics, University of Liverpool, Liverpool, L69 3BX, UK.

⁴Ningbo Institute of Digital Twin, Eastern Institute of Technology, Ningbo 315200, Zhejiang, China.

#Authors contributed equally.

*Correspondence to: Prof. Jinguang Hu, Department of Chemical and Petroleum Engineering, University of Calgary, 2500 University Drive, NW, Calgary, Alberta T2N 1N4, Canada. E-mail: jinguang.hu@ucalgary.ca; Prof. Heng Zhao, College of Engineering, Eastern Institute of Technology, 568 Tongxin Road, Ningbo 315200, Zhejiang, China. E-mail: hzhao@eitech.edu.cn; Prof. Zhangxing Chen, Ningbo Institute of Digital Twin, Eastern Institute of Technology, 568 Tongxin Road, Ningbo 315200, Zhejiang, China. E-mail: zxchen@eitech.edu.cn

How to cite this article: Yu, X.; Liu, D.; Fu, C.; Zhu, B.; Yong, X.; Hu, J.; Zhao, H.; Chen, Z. Bandgap engineering of $\text{Zn}_{1-x}\text{Cd}_x\text{S}$ for glycerol photo(electro)reforming into glyceric acid with hydrogen coproduction. *Chem. Synth.* 2025, 5, 48. <https://dx.doi.org/10.20517/cs.2024.136>

Received: 23 Sep 2024 **First Decision:** 5 Nov 2024 **Revised:** 29 Nov 2024 **Accepted:** 5 Dec 2024 **Published:** 14 May 2025

Academic Editor: Xiangdong Yao **Copy Editor:** Pei-Yun Wang **Production Editor:** Pei-Yun Wang

Abstract

The surplus of glycerol generation from biodiesel fuel production has stimulated the development of efficient technology to realize the sustainability of biomass valorization. Herein, we demonstrate the glycerol valorization by mild photocatalytic and photoelectrocatalytic approaches. Glycerol photo(electro)reforming is realized on the well-designed $\text{Zn}_{1-x}\text{Cd}_x\text{S}$ solid solution photocatalysts. By continuously changing the ratio of Zn/Cd, $\text{Zn}_{1-x}\text{Cd}_x\text{S}$ is endowed with a regulatable bandgap structure, which finely controls the redox potential and light absorption. The spontaneous formation of homojunction by hexagonal wurtzite (WZ) and zinc-blende (ZB) facilitates spatial charge separation. As a result, $\text{Zn}_{1-x}\text{Cd}_x\text{S}$ exhibits the dual ability to simultaneously produce hydrogen and glyceric acid by the electrons and holes, respectively. The theoretical calculation and *in-situ* spectroscopy analysis reveal the prominent features of hydrogen evolution and glycerol oxidation into glyceric acid on the optimized $\text{Zn}_{0.5}\text{Cd}_{0.5}\text{S}$. This work provides a good example for glycerol valorization into sustainable fuels and chemicals by rationally designing dually functional photocatalysts.

Keywords: Glycerol photo(electro)reforming, $\text{Zn}_{1-x}\text{Cd}_x\text{S}$, band gap engineering, hydrogen, glyceric acid



© The Author(s) 2025. **Open Access** This article is licensed under a Creative Commons Attribution 4.0 International License (<https://creativecommons.org/licenses/by/4.0/>), which permits unrestricted use, sharing, adaptation, distribution and reproduction in any medium or format, for any purpose, even commercially, as long as you give appropriate credit to the original author(s) and the source, provide a link to the Creative Commons license, and indicate if changes were made.



INTRODUCTION

Biomass valorization to produce value-added chemicals or fuels provides a sustainable alternative to release the pressure from the depletion of traditional fossil energy^[1-5]. Biodiesel fuel production from biomass valorization is one of the most mature technologies and its market demand is increasing annually^[6-8]. However, the production of biodiesel fuel is always accompanied by the coproduction of crude glycerol (~10% of glycerol) as a byproduct, and it is predicted that six million tons of glycerol will be produced in 2025^[9,10]. Due to the limited market size of glycerol, the valorization of glycerol to value-added chemicals and gas fuels has been attracting extensive attention^[11-13].

Steam reforming, pyrolysis and biological processes are the most common strategies for current glycerol conversion into gaseous and/or liquid products^[14-18]. However, these processes always suffer from high energy input and/or low product selectivity. Photocatalytic and photoelectrocatalytic glycerol utilization with solar energy, as the driving force, holds outstanding features of mild reaction conditions and high product selectivity^[19-23]. Currently, glycerol valorization by photo(electro)catalysis can be divided into two processes: photooxidation (with O₂) and photoreforming (without O₂). The former uses O₂ or species derived from O₂ as oxidants to convert glycerol, while the latter primarily uses glycerol as an electron donor to produce hydrogen^[24-27]. By photocatalysis, glycerol can be converted into a vast range of value-added liquid and gaseous products such as dihydroxyacetone, glyceraldehyde, glyceric acid, glycolic acid, CO and H₂ due to its highly functionalized nature from the three hydroxyl groups^[28-31]. Glyceric acid, the important intermediate for light industries, is commonly produced via selective oxidation of glycerol under alkali conditions and in presence of noble metals^[32-34]. Herein, rationally designing photocatalysts to achieve selective glyceric acid production from glycerol photo(electro)reforming along with sustainable H₂ production holds promising perspectives from industrial and academic points of view.

The fundamental process of glycerol photo(electro)reforming is that the photogenerated electrons reduce protons from glycerol or water to produce hydrogen while the glycerol as an electron donor releases protons and timely consumes the photogenerated holes^[35,36]. Improving the separation efficiency of photogenerated electrons and holes is apparently one of the approaches to boost glycerol conversion and hydrogen production. However, the selective glycerol conversion cannot be simultaneously guaranteed during the photo(electro)reforming process. As the redox ability of photocatalysts can be regulated by changing the band gap structure, it provides a possibility to selectively convert glycerol along with hydrogen coproduction by bandgap engineering strategy^[37]. Fine regulation of the band gap structure of semiconductors is a kind of challenge. Until now, quantum size effect and doping have been revealed as strategies to slightly change the band gap structure^[38,39]. However, these always involve complicated procedures and introduction of defects as recombination centers for electrons and holes^[40]. Solid solutions stand out because their band gap structure can be continuously regulated by changing the ratio of solute atoms in the solvent lattice^[41,42]. In particular, the cost-effective Zn_{1-x}Cd_xS, a typical solid solution, has been widely investigated as a photocatalyst due to tunable band structure and compositions of exposed crystal facets^[43-45]. Besides, the well-established homojunction structure by introducing twinning superlattice in Zn_{1-x}Cd_xS nanocrystal also realizes efficient charge separation to boost the quantum yield^[46,47]. Glycerol photoreforming has also been demonstrated over Zn_{1-x}Cd_xS but only with hydrogen production^[48]. The liquid or other gaseous products by photo(electro)reforming approach have not been systematically investigated to reveal the detailed reaction pathway.

Herein, to fill this gap, we design and fabricate a series of Zn_{1-x}Cd_xS photocatalysts with twinning superlattice and homojunction structure, which benefit the separation efficiency of photogenerated electrons and holes. The redox ability and visible light absorption capability can be continuously regulated

by changing the Cd/Zn ratio. Specifically, increasing the Cd/Zn ratio leads to enhanced visible light absorption, but the narrow bandgap structure is accompanied by limited redox ability. As a result, $\text{Zn}_{1-x}\text{Cd}_x\text{S}$ photocatalysts exhibit excellent H_2 production, which strongly depends on the Cd/Zn ratio. Glyceric acid is selectively produced from glycerol oxidation by the photogenerated holes. Besides, the glycerol photoelectroreforming test is also performed and $\text{Zn}_{0.5}\text{Cd}_{0.5}\text{S}$ exhibits good photoelectrocatalytic activity. This work demonstrates a good example for simultaneous production of gas fuels and value-added chemicals from glycerol photoreforming.

EXPERIMENTAL

Detailed experimental materials and methods were included in [Supplementary Materials](#).

RESULTS AND DISCUSSION

$\text{Zn}_{1-x}\text{Cd}_x\text{S}$ solid solutions with different Zn/Cd ratios were prepared by a hydrothermal process with zinc acetate dihydrate, cadmium acetate dihydrate and thioacetamide as precursors. The obtained samples exhibited different colors from white (ZnS) gradually to orange (CdS), indicating the enhanced visible light absorbance with the increasing cadmium content [Figure 1A]. The obtained $\text{Zn}_{1-x}\text{Cd}_x\text{S}$ solid solutions exhibited crystalline particles [Figure 1B and Supplementary Figure 1]. The high-angle annular dark-field scanning transmission electron microscopy (HAADF-STEM) image and corresponding elemental mappings reveal the uniform distribution of Zn, Cd and S in the crystals [Figure 1C]. High-resolution transmission electron microscopy (HRTEM) was performed to check the fine crystalline structure at an atomic scale. The presence of both hexagonal wurtzite (WZ) structure and cubic zinc-blende (ZB) could be clearly observed in a single crystalline particle [Figure 1D]. The phase boundary could also be clearly identified. The crystal structures are further confirmed by the fast Fourier transform (FFT) patterns [Figure 1E and F]. Meanwhile, ZB and WZ crystal phases are also observed in separated crystalline particles [Figure 1G and H], further indicating the presence of twin crystals inside this material. The twin boundaries are clearly identified, which benefits efficient charge separation [Figure 1I and Supplementary Figure 2]. Revealed by the energy dispersive X-ray spectroscopy (EDS) elemental mappings, Zn, Cd and S atoms are homogeneously distributed even on the atomic scale, which is the characteristic feature of solid solution [inset of Figure 1I and Supplementary Figure 3].

The change in crystal structure with different Zn/Cd ratios was tracked by X-ray diffraction [Figure 2A]. It is obvious that ZnS exhibits a typical cubic ZB crystal phase (JCPDS Card: 03-065-1691). With the introduction of Cd to gradually replace Zn in $\text{Zn}_{1-x}\text{Cd}_x\text{S}$ solid solutions, the crystal structure changes from cubic ZB phase to hexagonal WZ phase with a significant shift to a smaller diffraction angle of pristine ZnS (110) plane. Typical hexagonal WZ diffraction peaks at 24.8° , 26.4° and 28.2° are identified for pure CdS (100), (002) and (101) planes, respectively. Noticeably, the relative peak intensity of (002) of as-fabricated CdS is extremely higher than that of the reference pattern (JCPDS Card No. 01-077-2306), which is ascribed to the presence of cubic ZB crystal phase in CdS. The existence of a cubic phase in CdS could further be revealed by the diffraction peak at 30.5° , which corresponds to the (200) plane of cubic ZB CdS. The above results clearly demonstrate the formation of homojunction structure within $\text{Zn}_{1-x}\text{Cd}_x\text{S}$ solid solutions by random cubic ZB phase and hexagonal WZ phase. Another advantage of solid solution photocatalysts is their continuously adjustable bandgap structure with different constituents. All the photocatalysts exhibit direct semiconductor properties and pure ZnS shows the ability to only absorb ultraviolet (UV) light with an absorption edge at 332 nm [Figure 2B]. With the increasing loading of Cd to gradually replace Zn atoms, $\text{Zn}_{1-x}\text{Cd}_x\text{S}$ solid solutions show redshifts in light absorption edge, and pure CdS exhibits an absorption edge at 518 nm. According to Kubelka-Munk theory, the corresponding band gaps are 3.73, 3.10, 2.67, 2.53 and 2.39 eV for ZnS, $\text{Zn}_{0.75}\text{Cd}_{0.25}\text{S}$, $\text{Zn}_{0.5}\text{Cd}_{0.5}\text{S}$, $\text{Zn}_{0.25}\text{Cd}_{0.75}\text{S}$ and CdS, respectively [Figure 2C].

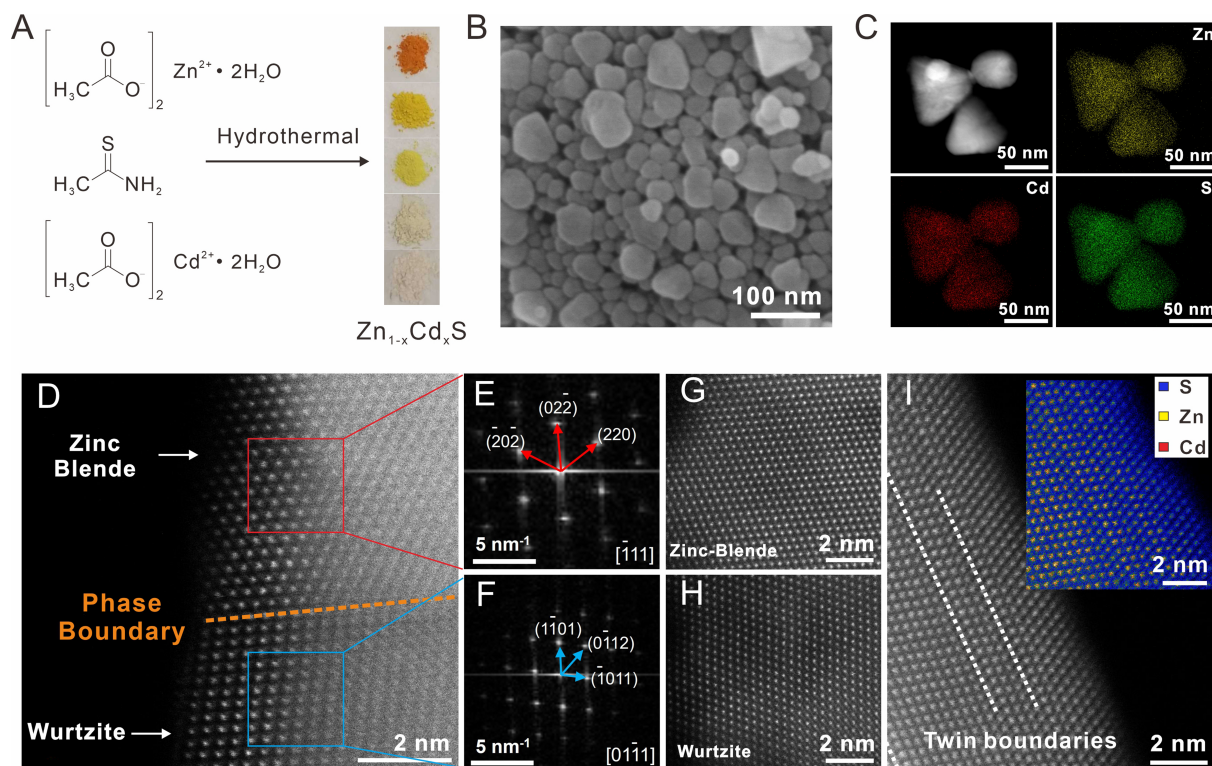


Figure 1. (A) Schematic illustration of Zn_{1-x}Cd_xS preparation; (B) a typical TEM image of Zn_{0.5}Cd_{0.5}S; (C) HAADF-STEM and corresponding elemental mappings of Zn_{0.5}Cd_{0.5}S; HR-TEM images of (D) WZ phase and ZB phase in a single crystal, (E) and (F) FFT patterns in the selected areas in (D); (G) ZB phase crystal and (H) WZ phase crystal; (I) HR-TEM image with the labeling of twin boundaries and elemental mappings at the atomic scale (inset). TEM: Transmission electron microscopy; HAADF-STEM: high-angle annular dark-field scanning transmission electron microscopy; HR-TEM: high-resolution transmission electron microscopy; WZ: wurtzite; ZB: zinc-blende; FFT: fast Fourier transform.

To clarify the exact positions of the bandgap structure of Zn_{1-x}Cd_xS solid solutions, Mott-Schottky plots are recorded in a typical three-electrode system with photocatalyst on fluorine-doped tin oxide (FTO) as the working electrode, a Pt plate as the counter electrode and Ag/AgCl as the reference electrode. All the Zn_{1-x}Cd_xS solid solutions exhibit n-type semiconductor properties and the detected flat potentials are -1.08, -0.95, -0.90, -0.70 and -0.41 V vs. Ag/AgCl for ZnS, Zn_{0.75}Cd_{0.25}S, Zn_{0.5}Cd_{0.5}S, Zn_{0.25}Cd_{0.75}S and CdS, respectively [Figure 2D]. Valence band X-ray photoelectron spectroscopy (VB-XPS) was then performed to determine the valence band potentials combined with Mott-Schottky results, which are calculated to be 1.01, 0.98, 1.31, 1.21 and 1.47 V vs. normal hydrogen electrode (NHE) for ZnS, Zn_{0.75}Cd_{0.25}S, Zn_{0.5}Cd_{0.5}S, Zn_{0.25}Cd_{0.75}S and CdS, respectively [Supplementary Figure 4]. Combining the band gaps from UV-visible diffuse reflectance spectra, the bandgap structures of Zn_{1-x}Cd_xS solid solutions are illustrated accordingly [Figure 2E]. Increasing the cadmium content in Zn_{1-x}Cd_xS solid solutions improves visible light absorbance but sacrifices redox ability. The chemical state on the Zn_{1-x}Cd_xS surface was investigated by X-ray photoelectron spectroscopy (XPS) and all the results have been calibrated by C 1s at 284.8 eV. Characteristic peaks of Zn, Cd and S were shown in XPS survey spectra [Supplementary Figure 5]. Carbon and oxygen were also observed, which should come from the adventitious hydrocarbon in the equipment. The two typical peaks with splitting energy of 23.0 eV in high-resolution XPS spectra of Zn 2p indicate that the Zn element exists as Zn²⁺ [Figure 2F]. The binding energies of Zn 2p_{3/2} and Zn 2p_{1/2} gradually shift to higher values with increasing Cd content, which is attributed to the higher electronegativity of Cd (1.7) than that of Zn (1.6) and the cubic structure of all the Zn-S chemical bonds. In contrast, the binding energies of Cd 3d_{5/2} and Cd 3d_{3/2} first shift to higher values and then lower values with gradually increasing Cd content

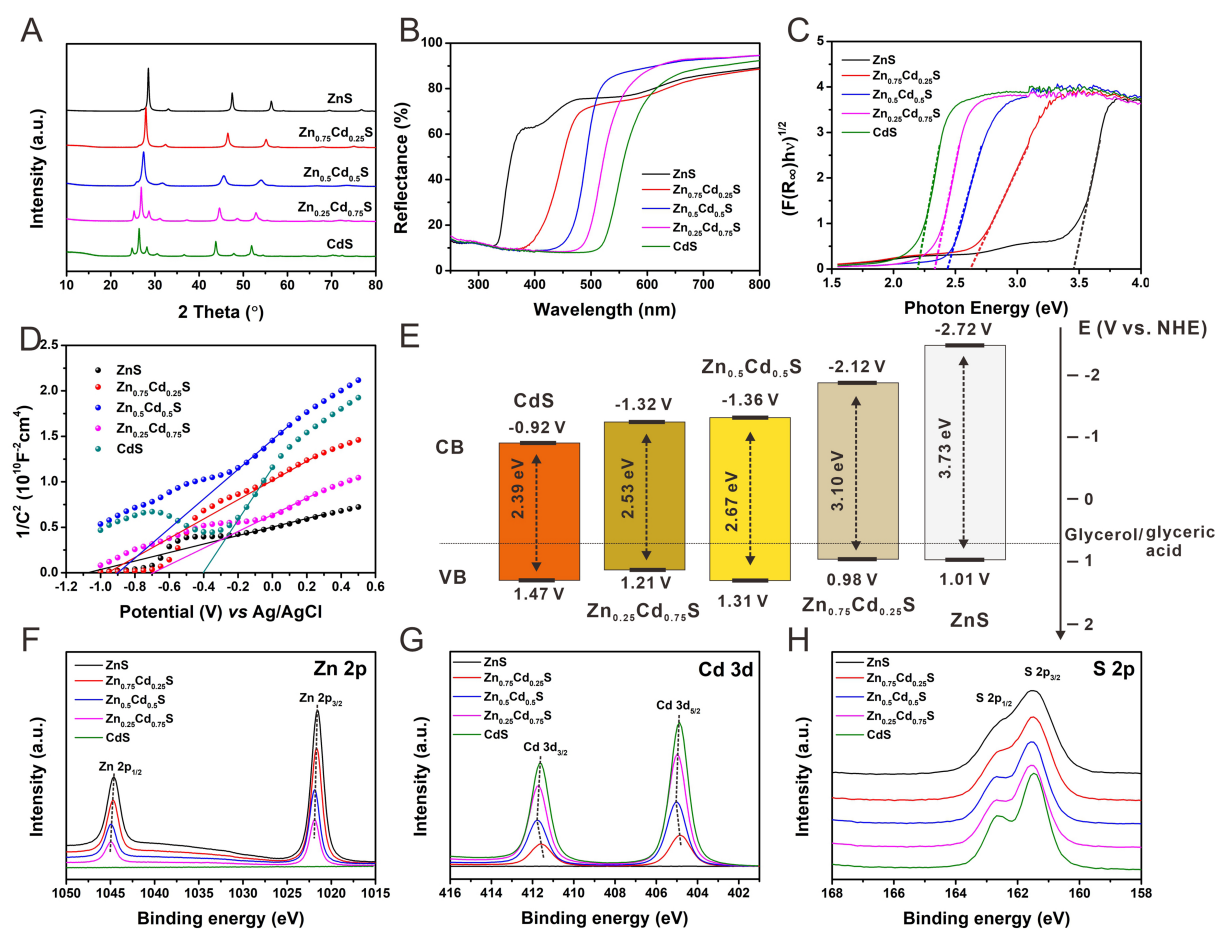


Figure 2. (A) XRD patterns, (B) UV-vis diffuse reflectance spectra, (C) Tauc plots, (D) Mott-Schottky plots and (E) bandgap structures illustration of $\text{Zn}_{1-x}\text{Cd}_x\text{S}$ solid solutions; High-resolution XPS spectra of (F) Zn 2p, (G) Cd 3d and (H) S 2p of $\text{Zn}_{1-x}\text{Cd}_x\text{S}$ solid solutions. XRD: X-ray diffraction; UV-vis: ultraviolet-visible; XPS: X-ray photoelectron spectroscopy.

[Figure 2G], which is due to the synergistic effect of electronegativity and formation of homojunction by cubic and hexagonal structures. The crystal structure of Cd-S chemical bonds mainly exists in cubic structures with low Cd content and hexagonal structure dominants with high Cd content [Figure 2A]. The two typical S 2p_{3/2} and S 2p_{1/2} peaks indicate the S²⁻ in $\text{Zn}_{1-x}\text{Cd}_x\text{S}$ solid solutions [Figure 2H].

The photocatalytic activity of as-prepared $\text{Zn}_{1-x}\text{Cd}_x\text{S}$ solid solutions was evaluated by glycerol photoreforming. Pristine $\text{Zn}_{1-x}\text{Cd}_x\text{S}$ solid solutions without any cocatalyst were first investigated for H₂ evolution. All the samples exhibited almost linear relation of H₂ amount with reaction time and the Zn/Cd ratio greatly affected the photocatalytic performance [Figure 3A]. Compared with bare CdS, with addition of Zn in crystal structure, samples exhibited significantly enhanced H₂ production. This should be attributed to the formation of solid solution structure, which facilitates the spontaneously separation of photogenerated electrons and holes. This could be revealed by the enhanced photocurrent density and reduced electrochemical impedance of $\text{Zn}_{0.5}\text{Cd}_{0.5}\text{S}$ compared to pristine CdS [Supplementary Figure 6]. Noticeably, a negligible amount of CO was also detected without any CO₂ generation [Supplementary Figure 7]. The H₂ evolution in the presence of Pt photodeposition still exhibited a linear relation with reaction time [Figure 3B]. The formation of a Schottky junction through *in-situ* introduction of Pt as a cocatalyst further boosted the photocatalytic H₂ production for all the $\text{Zn}_{1-x}\text{Cd}_x\text{S}$ samples, except for ZnS, which is a UV-responsible material. Differently, $\text{Zn}_{0.75}\text{Cd}_{0.25}\text{S}$ exhibited the highest H₂ generation rate

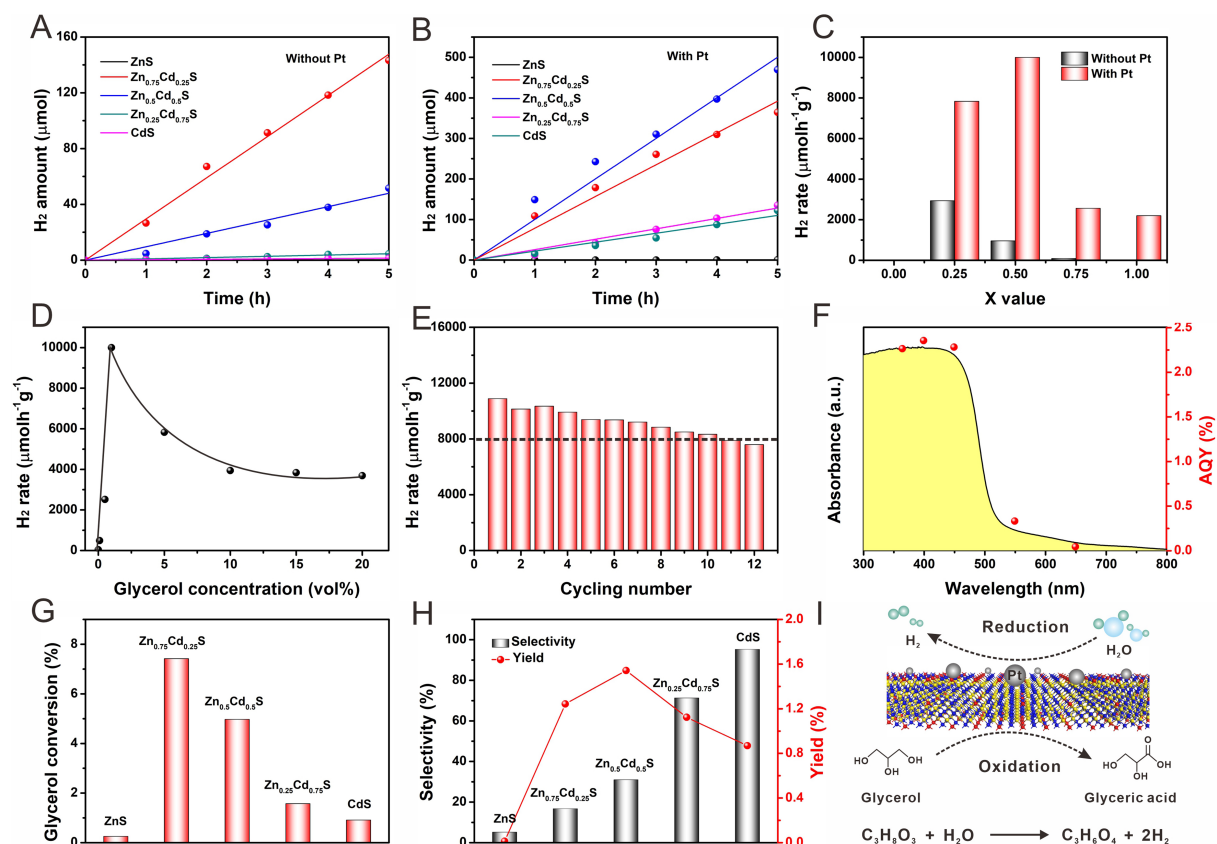


Figure 3. Photocatalytic H₂ generation of Zn_{1-x}Cd_xS solid solutions from glycerol solution (A) without and (B) with Pt as cocatalyst, (C) corresponding H₂ generation rates; (D) H₂ generation of Zn_{0.5}Cd_{0.5}S with Pt from different glycerol concentration; (E) cycling test of Zn_{0.5}Cd_{0.5}S; (F) light absorbance spectrum of Zn_{0.5}Cd_{0.5}S and calculated AQY values at different monochromatic lights; (G) glycerol conversion, (H) glyceric acid selectivity and yield of Zn_{1-x}Cd_xS solid solutions, (I) proposed reaction mechanism. AQY: Apparent quantum yield.

(2.94 mmol·h⁻¹·g⁻¹) without Pt while Zn_{0.5}Cd_{0.5}S showed the best performance (10.0 mmol·h⁻¹·g⁻¹) with Pt as cocatalyst [Figure 3C]. Three major factors that affect photocatalytic H₂ production are light absorption region (bandgap width), charge separation and redox potential. Zn_{0.5}Cd_{0.5}S with Pt may synergistically maximize these factors to achieve the best performance for H₂ production. The Zn_{0.5}Cd_{0.5}S and Zn_{0.75}Cd_{0.25}S were collected after photocatalytic reaction with the deposition of Pt for the determination of Pt loading and distribution. The inductively coupled plasma-atomic emission spectrometry (ICP-AES) revealed the similar atomic loading of Pt on Zn_{0.5}Cd_{0.5}S (0.11%) and Zn_{0.75}Cd_{0.25}S (0.13%), respectively. However, the distribution of Pt was found to be totally different from TEM images and corresponding elemental mappings [Supplementary Figure 8]. A significant aggregation of Pt could be found in Zn_{0.5}Cd_{0.5}S while high dispersion of Pt was on Zn_{0.75}Cd_{0.25}S with no aggregation of Pt, which probably originates from the stronger redox ability of Zn_{0.75}Cd_{0.25}S than Zn_{0.5}Cd_{0.5}S, inducing the fast deposition of Pt from H₂PtCl₆ precursors. The effect of glycerol concentration on photocatalytic H₂ generation was also investigated [Figure 3D]. The optimized glycerol concentration was found to be 1% in volume. Lower glycerol concentration is inefficient in consuming the photogenerated holes while higher glycerol concentration would affect the light penetration due to its high viscosity. The photocatalytic stability of Zn_{0.5}Cd_{0.5}S was evaluated during the long-time cycling test [Figure 3E]. A slight decrease in photocatalytic performance was observed but H₂ generation rate was almost maintained at 8.00 mmol·h⁻¹·g⁻¹, indicating the relatively good stability of as-prepared photocatalysts. The apparent quantum yield (AQY) was then investigated on Zn_{0.5}Cd_{0.5}S samples at

different monochromatic lights. The AQY values follow well with the UV-visible light absorption profile and reach around 2.27%, 2.36%, 2.28% at the wavelengths of 365, 400, 450 nm, respectively [Figure 3F]. The glycerol conversion and liquid phase products were also monitored along with H_2 production. Glycerol conversion is not only related to the charge separation efficiency but also attributed to the oxidation potential of photocatalysts. With increasing Zn content, $Zn_{1-x}Cd_xS$ samples exhibited enhanced glycerol conversion and $Zn_{0.75}Cd_{0.25}S$ showed highest performance ($\sim 7.40\%$ within 5 h), which is consistent with the improved oxidation ability [Figure 3G and 2E]. Glyceric acid was the main liquid product determined by HPLC with some other side products such as dihydroxyacetone [Supplementary Figure 9]. Its selectivity gradually increased with the Cd ratio [Figure 3H] and pure CdS exhibited the highest glyceric acid selectivity ($\sim 95\%$). The possible reaction pathway of glycerol photoreforming into glyceric acid was proposed based on the detected liquid products [Supplementary Figure 10]. Limited by the low glycerol conversion, the yield of glyceric acid was not significant. However, $Zn_{0.5}Cd_{0.5}S$ still showed the best performance for glyceric acid production. The developed $Zn_{0.5}Cd_{0.5}S$ delivers comparable activity for photocatalytic glycerol valorization and hydrogen production compared to the literature [Supplementary Table 1]. The reaction pathway was herein proposed [Figure 3I]. Under the irradiation of visible light, $Zn_{1-x}Cd_xS$ photocatalysts are activated to produce electrons and holes. The presence of Pt nanoparticles on the surface traps the photogenerated electrons to reduce protons to produce H_2 while the photogenerated holes oxidize the absorbed glycerol into glyceric acid.

The photoelectrocatalytic performance was then investigated for $Zn_{0.5}Cd_{0.5}S$ as it showed the compromised activity for both H_2 production and glycerol oxidation. The film on FTO was endowed with a similar morphology of $Zn_{0.5}Cd_{0.5}S$ compared to the powder but with significantly reduced crystal sizes. The thickness was measured to be around $1.08\ \mu m$ [Supplementary Figure 11]. The variables of light irradiation and glycerol were applied for this test. The photocurrent densities were extremely low under dark conditions even with the addition of glycerol [Figure 4A]. Under the light irradiation, $Zn_{0.5}Cd_{0.5}S$ exhibited an enhanced photocurrent density for water splitting and the photocurrent density was boosted to $1.12\ mA/cm^2$ at $1.23\ V$ vs. reversible hydrogen electrode (RHE) in the absence of glycerol, which is attributed to charge separation of the photogenerated electrons and holes. With the addition of glycerol, the photocurrent density was further increased to $5.90\ mA/cm^2$ at $1.23\ V$ vs. RHE, indicating the enhanced H_2 generation on the photocathode by coupling glycerol oxidation on the photoanode. The transient response and durability of $Zn_{0.5}Cd_{0.5}S$ photoelectrode were then investigated over several on-off irradiation cycles [Figure 4B]. The photocurrent rapidly increased to a constant value when the light was turned on while it instantly decreased to almost zero when the light was turned off, indicating the excellent transient response of the as-fabricated photoelectrode. The high durability of $Zn_{0.5}Cd_{0.5}S$ photoelectrodes could be revealed by the stable photocurrent density under light irradiation and the photographs [Figure 4B and C]. After 5 h reaction, 6.71% glycerol conversion was achieved with 40.3% glyceric acid selectivity, which was enhanced from 4.97% glycerol conversion and 31.0% glyceric acid selectivity by photocatalysis, indicating the prominent contribution of photoelectrocatalysis [Figure 4D].

The theoretical calculation revealed that bandgap energies were 2.44, 1.76, 1.38, 1.11 and 1.05 eV for ZnS, $Zn_{0.75}Cd_{0.25}S$, $Zn_{0.5}Cd_{0.5}S$, $Zn_{0.25}Cd_{0.75}S$ and CdS respectively [Figure 5A-E and Supplementary Figure 12]. The calculated bandgap energies were smaller than those obtained from UV-visible diffuse reflectance spectra but with a consistent trend of decline compared to the measured results. Subsequently, the hydrogen evolution reaction (HER) processes of five proportionally corresponding structures under the neutral condition were simulated [Figure 5F]. The effect of proton adsorption sites on free energy was also investigated on $Zn_{0.75}Cd_{0.25}S$, $Zn_{0.5}Cd_{0.5}S$ and $Zn_{0.25}Cd_{0.75}S$. Pristine ZnS ($\Delta G = 0.46\ eV$) delivered smaller HER free energy than CdS ($\Delta G = 0.66\ eV$). However, the activity of the Cd site ($\Delta G = 0.21\ eV$) in $Zn_{0.25}Cd_{0.75}S$

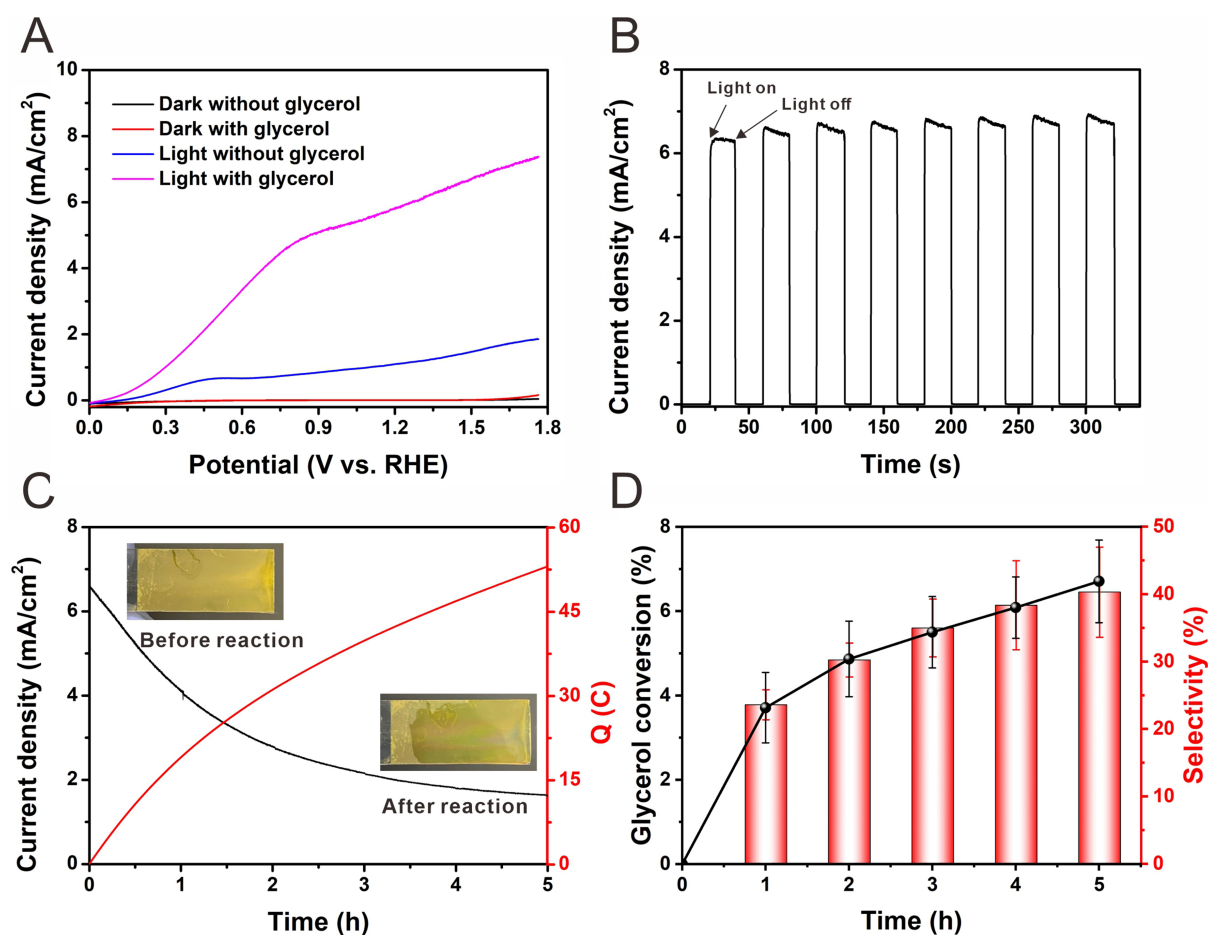


Figure 4. (A) LSV curves of $\text{Zn}_{0.5}\text{Cd}_{0.5}\text{S}$ in 0.1 M KOH solution with and without glycerol under dark and Xenon lamp illumination; (B) Transient response to the light irradiation at 1.2 V vs. RHE in 0.1 M KOH solution with 0.1 M glycerol; (C) Photocurrent density and calculated charge with increasing reaction time (insets are the photos of the working electrode before and after reaction; (D) Glycerol conversion and glyceric acid selectivity. LSV: Linear sweep voltammetry; RHE: reversible hydrogen electrode.

material was smaller than that of the Zn site ($\Delta G = 1.90$ eV). In the comparison of $\text{Zn}_{0.75}\text{Cd}_{0.25}\text{S}$ and $\text{Zn}_{0.5}\text{Cd}_{0.5}\text{S}$, the Zn site was superior to the Cd site, with values of 0.10 and 0.24 eV corresponding to the Zn site and 0.26 and 0.37 eV corresponding to the Cd site, respectively. The change of HER free energy of $\text{Zn}_{0.75}\text{Cd}_{0.25}\text{S}$ catalysts was closest to 0 eV, indicating its best hydrogen production performance under neutral conditions, which was consistent with the experimental result. The selective glycerol oxidation into glyceric acid revealed that additional energy was required for the dehydrogenation steps on the primary carbon atom, which were key steps in the whole oxidation reaction [Figure 5G]. The free energy change was up to 0.50 eV for the C-H breakage on $\text{Zn}_{0.5}\text{Cd}_{0.5}\text{S}$, while the release of a second hydrogen atom from the carbon required 0.70 eV on $\text{Zn}_{0.75}\text{Cd}_{0.25}\text{S}$, which was much higher than that on $\text{Zn}_{0.5}\text{Cd}_{0.5}\text{S}$. The theoretical calculation results supported the experiment that $\text{Zn}_{0.5}\text{Cd}_{0.5}\text{S}$ delivered the best yield of glyceric acid from glycerol oxidation.

The density of states was further analyzed to confirm the prominent features of $\text{Zn}_{0.5}\text{Cd}_{0.5}\text{S}$ in the whole oxidation process of glycerol into glyceric acid. For the first dehydrogenation step on the primary carbon atom of glycerol, the O2p orbital was a major part of bonding to the Zn3d orbital in $\text{Zn}_{0.75}\text{Cd}_{0.25}\text{S}$ and $\text{Zn}_{0.5}\text{Cd}_{0.5}\text{S}$, in which the occupation energy in $\text{Zn}_{0.75}\text{Cd}_{0.25}\text{S}$ was slightly lower than that in $\text{Zn}_{0.5}\text{Cd}_{0.5}\text{S}$.

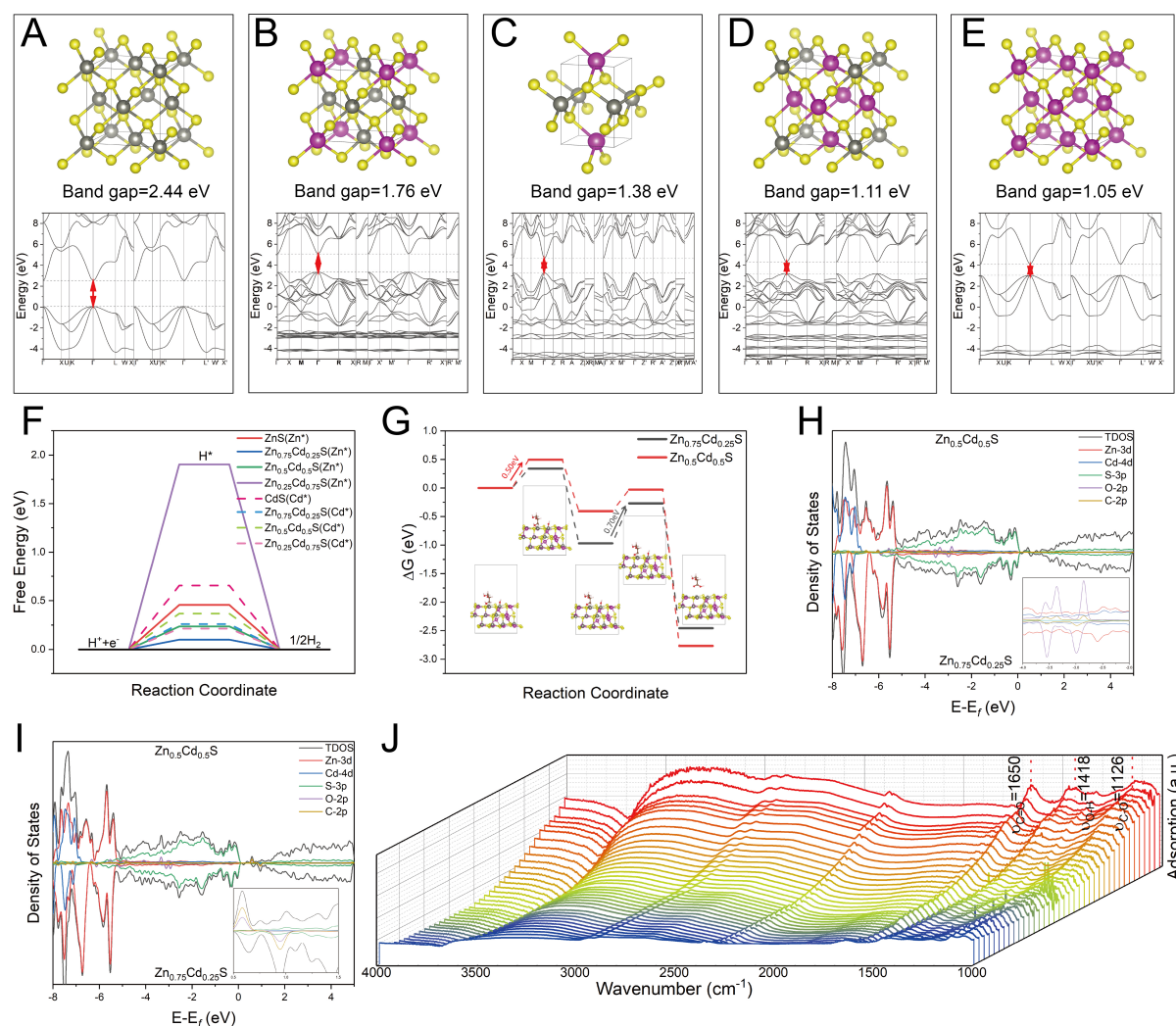


Figure 5. Band structure and atomic illustrations of $\text{Zn}_{1-x}\text{Cd}_x\text{S}$: (A) ZnS, (B) $\text{Zn}_{0.75}\text{Cd}_{0.25}\text{S}$, (C) $\text{Zn}_{0.5}\text{Cd}_{0.5}\text{S}$, (D) $\text{Zn}_{0.25}\text{Cd}_{0.75}\text{S}$, (E) CdS, (F) the HER step-chart of $\text{Zn}_{1-x}\text{Cd}_x\text{S}$ with (111) facet, (G) oxidation of glycerol with $\text{Zn}_{0.75}\text{Cd}_{0.25}\text{S}$ and $\text{Zn}_{0.5}\text{Cd}_{0.5}\text{S}$ and corresponding structure inset; (H) and (I) Density of states graphs for first and second dehydrogenation step; (J) *In situ* DRIFTS spectra of glycerol oxidation on $\text{Zn}_{0.5}\text{Cd}_{0.5}\text{S}$ surface. HER: Hydrogen evolution reaction; DRIFTS: diffuse reflectance infrared Fourier transform spectroscopy.

[Figure 5H]. For the second dehydrogenation step, the emergence of C2p and O2p orbital above the fermi level region indicates the formation of anti-bonding orbital in C-O linkage, which made the second dehydrogenation step as the rate-determining step of glycerol oxidation into glyceric acid [Figure 5I]. Noticeably, $\text{Zn}_{0.5}\text{Cd}_{0.5}\text{S}$ delivered a lower anti-bonding energy than $\text{Zn}_{0.75}\text{Cd}_{0.25}\text{S}$, making it an ideal photocatalyst in $\text{Zn}_{1-x}\text{Cd}_x\text{S}$ for glycerol conversion into glyceric acid. *In situ* diffuse reflectance infrared Fourier transform spectroscopy (DRIFTS) was performed to monitor the reaction pathway of glycerol oxidation into glyceric acid [Figure 5J]. The Fourier transform spectroscopy (FTIR) spectra in the 1,114–1,126 cm^{-1} region corresponded to a bridging alkoxy bond formed from one primary alcohol group of glycerol and two metal surface atoms^[49]. The symmetric stretch $\nu(\text{OCO})$ of twofold carboxylate species appeared at 1,418 cm^{-1} ^[50]. The band centered at 1,650 cm^{-1} corresponded to the $\nu(\text{C}=\text{O})$ stretch mode of adsorbed aldehyde species, indicating the oxidation of hydroxyl group into carboxyl group of glycerol^[51].

CONCLUSIONS

In summary, $\text{Zn}_{1-x}\text{Cd}_x\text{S}$ solid solutions have been successfully synthesized with bandgap engineering for glycerol photoreforming. The changeable bandgap structure regulates redox potential and light absorption. The spontaneous formation of homojunction by hexagonal WZ and ZB facilitates spatial charge separation. As a result, a considerable amount of H_2 is produced by photogenerated electrons while glycerol is selectively oxidized into glyceric acid by the photogenerated holes. The as-fabricated material also exhibits excellent performance in glycerol photoelectroreforming process. This present work demonstrates an example for glycerol valorization into sustainable H_2 along with value-added chemicals coproduction by mild photo(electro)catalytic technology.

DECLARATIONS

Authors' contributions

Made substantial contributions to conception and design of the study, performed data analysis and interpretation, and wrote the draft of the manuscript: Yu, X.; Liu, D.; Zhu, B.

Performed DFT calculation: Fu, C.; Yong, X.

Discussed and revised the manuscript: Hu, J.; Zhao, H.; Chen, Z.

Availability of data and materials

Detailed experimental materials and methods were included in [Supplementary Materials](#), and the data supporting the findings of this study are available within its [Supplementary Materials](#).

Financial support and sponsorship

This work was financially supported by the Canada First Research Excellence Fund (CFREF) and research funding from the Ningbo Institute of Digital Twin, Eastern Institute of Technology, Ningbo.

Conflicts of interest

All authors declared that there are no conflicts of interest.

Ethical approval and consent to participate

Not applicable.

Consent for publication

Not applicable.

Copyright

© The Author(s) 2025.

REFERENCES

1. Liu, Z.; Wang, K.; Chen, Y.; Tan, T.; Nielsen, J. Third-generation biorefineries as the means to produce fuels and chemicals from CO_2 . *Nat. Catal.* **2020**, 3, 274-88. [DOI](#)
2. Song, B.; Lin, R.; Lam, C. H.; Wu, H.; Tsui, T.; Yu, Y. Recent advances and challenges of inter-disciplinary biomass valorization by integrating hydrothermal and biological techniques. *Renew. Sustain. Energy. Rev.* **2021**, 135, 110370. [DOI](#)
3. Sun, Z.; Zhao, H.; Yu, X.; Hu, J.; Chen, Z. Glucose photorefinery for sustainable hydrogen and value-added chemicals coproduction. *Chem. Synth.* **2024**, 4, 4. [DOI](#)
4. Ma, J.; Liu, K.; Yang, X.; et al. Recent advances and challenges in photoreforming of biomass-derived feedstocks into hydrogen, biofuels, or chemicals by using functional carbon nitride photocatalysts. *ChemSusChem* **2021**, 14, 4903-22. [DOI](#) [PubMed](#)
5. Shi, C.; Kang, F.; Zhu, Y.; et al. Photoreforming lignocellulosic biomass for hydrogen production: optimized design of photocatalyst and photocatalytic system. *Chem. Eng. J.* **2023**, 452, 138980. [DOI](#)
6. Yu, J.; Dappozze, F.; Martín-gomez, J.; et al. Glyceraldehyde production by photocatalytic oxidation of glycerol on WO_3 -based materials. *Appl. Catal. B. Environ.* **2021**, 299, 120616. [DOI](#)

7. Goh, B. H. H.; Chong, C. T.; Ge, Y.; et al. Progress in utilisation of waste cooking oil for sustainable biodiesel and biojet fuel production. *Energy. Convers. Manag.* **2020**, *223*, 113296. DOI
8. Sun, C.; Hu, Y.; Sun, F.; et al. Comparison of biodiesel production using a novel porous Zn/Al/Co complex oxide prepared from different methods: physicochemical properties, reaction kinetic and thermodynamic studies. *Renew. Energy*. **2022**, *181*, 1419-30. DOI
9. Stelmachowski, M.; Marchwicka, M.; Grabowska, E.; Diak, M. The photocatalytic conversion of (biodiesel derived) glycerol to hydrogen - a short review and preliminary experimental results part 1: a review. *J. Adv. Oxid. Technol.* **2014**, *17*, 167-78. DOI
10. Ciriminna, R.; Pina, C. D.; Rossi, M.; Pagliaro, M. Understanding the glycerol market. *Eur. J. Lipid. Sci. Technol.* **2014**, *116*, 1432-9. DOI
11. Estahbanati MR, Feilizadeh M, Attar F, Iliuta MC. Current developments and future trends in photocatalytic glycerol valorization: process analysis. *React. Chem. Eng.* **2021**, *6*, 197-219. DOI
12. Luo, L.; Chen, W.; Xu, S. M.; et al. Selective photoelectrocatalytic glycerol oxidation to dihydroxyacetone via enhanced middle hydroxyl adsorption over a Bi₂O₃-incorporated catalyst. *J. Am. Chem. Soc.* **2022**, *144*, 7720-30. DOI
13. Liu, D.; Liu, J. C.; Cai, W.; et al. Selective photoelectrochemical oxidation of glycerol to high value-added dihydroxyacetone. *Nat. Commun.* **2019**, *10*, 1779. DOI PubMed PMC
14. Saidi, M.; Moradi, P. Conversion of biodiesel synthesis waste to hydrogen in membrane reactor: theoretical study of glycerol steam reforming. *Int. J. Hydrogen. Energy*. **2020**, *45*, 8715-26. DOI
15. Bivona, L. A.; Vivian, A.; Fusaro, L.; Fiorilli, S.; Aprile, C. Design and catalytic applications of 1D tubular nanostructures: improving efficiency in glycerol conversion. *Appl. Catal. B. Environ.* **2019**, *247*, 182-90. DOI
16. Morales, D. M.; Jambrec, D.; Kazakova, M. A.; et al. Electrocatalytic conversion of glycerol to oxalate on Ni oxide nanoparticles-modified oxidized multiwalled carbon nanotubes. *ACS. Catal.* **2022**, *12*, 982-92. DOI
17. Chen, J.; Yan, S.; Zhang, X.; Tyagi, R. D.; Surampalli, R. Y.; Valéro, J. R. Chemical and biological conversion of crude glycerol derived from waste cooking oil to biodiesel. *Waste. Manag.* **2018**, *71*, 164-75. DOI
18. Tran, N. H.; Kannangara, G. S. Conversion of glycerol to hydrogen rich gas. *Chem. Soc. Rev.* **2013**, *42*, 9454-79. DOI PubMed
19. Lakshmana Reddy, N.; Cheralathan, K. K.; Durga Kumari, V.; Neppolian, B.; Muthukonda Venkatakrishnan, S. Photocatalytic reforming of biomass derived crude glycerol in water: a sustainable approach for improved hydrogen generation using Ni(OH)₂ decorated TiO₂ nanotubes under solar light irradiation. *ACS. Sustain. Chem. Eng.* **2018**, *6*, 3754-64. DOI
20. Zhao, S.; Dai, Z.; Guo, W.; Chen, F.; Liu, Y.; Chen, R. Highly selective oxidation of glycerol over Bi/Bi_{3.64}Mo_{0.36}O_{6.55} heterostructure: dual reaction pathways induced by photogenerated ¹O₂ and holes. *Appl. Catal. B. Environ.* **2019**, *244*, 206-14. DOI
21. Shen, Y.; Mamakhel, A.; Liu, X.; et al. Promotion mechanisms of Au supported on TiO₂ in thermal- and photocatalytic glycerol conversion. *J. Phys. Chem. C* **2019**, *123*, 19734-41. DOI
22. Zhang, Z.; Wang, M.; Zhou, H.; Wang, F. Surface sulfate ion on CdS catalyst enhances syngas generation from biopolyols. *J. Am. Chem. Soc.* **2021**, *143*, 6533-41. DOI
23. Chang, J.; Song, F.; Hou, Y.; et al. Molybdenum, tungsten doped cobalt phosphides as efficient catalysts for coproduction of hydrogen and formate by glycerol electrolysis. *J. Colloid. Interface. Sci.* **2024**, *665*, 152-62. DOI
24. Estahbanati, M. K.; Feilizadeh, M.; Iliuta, M. C. Photocatalytic valorization of glycerol to hydrogen: optimization of operating parameters by artificial neural network. *Appl. Catal. B. Environ.* **2017**, *209*, 483-92. DOI
25. Guo, L.; Sun, Q.; Marcus, K.; et al. Photocatalytic glycerol oxidation on Au_xCu-CuS@TiO₂ plasmonic heterostructures. *J. Mater. Chem. A*. **2018**, *6*, 22005-12. DOI
26. Xiao, Y.; Wang, M.; Liu, D.; et al. Selective photoelectrochemical oxidation of glycerol to glyceric acid on (002) facets exposed WO₃ nanosheets. *Angew. Chem. Int. Ed. Engl.* **2024**, *63*, e202319685. DOI
27. Yu, X.; Yu, Z.; Zhao, H.; Gates, I. D.; Hu, J. Photothermal catalytic H₂ production over hierarchical porous CaTiO₃ with plasmonic gold nanoparticles. *Chem. Synth.* **2023**, *3*, 3. DOI
28. Ouyang, J.; Liu, X.; Wang, B. H.; et al. WO₃ photoanode with predominant exposure of {202} facets for enhanced selective oxidation of glycerol to glyceraldehyde. *ACS. Appl. Mater. Interfaces*. **2022**, *23*, 23536-45. DOI
29. Lu, Y.; Lee, B. G.; Lin, C.; et al. Solar-driven highly selective conversion of glycerol to dihydroxyacetone using surface atom engineered BiVO₄ photoanodes. *Nat. Commun.* **2024**, *15*, 5475. DOI PubMed PMC
30. Yu, J.; González-Cobos, J.; Dappozze, F.; et al. WO₃-based materials for photoelectrocatalytic glycerol upgrading into glyceraldehyde: unravelling the synergistic photo- and electro-catalytic effects. *Appl. Catal. B. Environ.* **2022**, *318*, 121843. DOI
31. Kim, D.; Oh, L. S.; Tan, Y. C.; Song, H.; Kim, H. J.; Oh, J. Enhancing glycerol conversion and selectivity toward glycolic acid via precise nanostructuring of electrocatalysts. *ACS. Catal.* **2021**, *11*, 14926-31. DOI
32. Carrettin, S.; McMorn, P.; Johnston, P.; Griffin, K.; Hutchings, G. J. Selective oxidation of glycerol to glyceric acid using a gold catalyst in aqueous sodium hydroxide. *Chem. Commun.* **2002**, 696-7. DOI
33. Zhang, X.; Zhou, D.; Wang, X.; et al. Overcoming the deactivation of Pt/CNT by introducing CeO₂ for selective base-free glycerol-to-glyceric acid oxidation. *ACS. Catal.* **2020**, *10*, 3832-7. DOI
34. Yan, H.; Yao, S.; Zhao, S.; et al. Insight into the basic strength-dependent catalytic performance in aqueous phase oxidation of glycerol to glyceric acid. *Chem. Eng. Sci.* **2021**, *230*, 116191. DOI
35. Sanwald, K. E.; Berto, T. F.; Jentys, A.; Camaioni, D. M.; Gutiérrez, O. Y.; Lercher, J. A. Kinetic coupling of water splitting and photoreforming on SrTiO₃-based photocatalysts. *ACS. Catal.* **2018**, *8*, 2902-13. DOI
36. Li, Y.; Zhang, D.; Qiao, W.; et al. Nanostructured heterogeneous photocatalyst materials for green synthesis of valuable chemicals.

- Chem. Synth. 2022, 2, 9. DOI
37. Lin, J.; Wu, X.; Xie, S.; et al. Visible-light-driven cleavage of C-O linkage for lignin valorization to functionalized aromatics. *ChemSusChem* 2019, 12, 5023-31. DOI
38. Holmes, M. A.; Townsend, T. K.; Osterloh, F. E. Quantum confinement controlled photocatalytic water splitting by suspended CdSe nanocrystals. *Chem. Commun.* 2012, 48, 371-3. DOI PubMed
39. Asahi, R.; Morikawa, T.; Irie, H.; Ohwaki, T. Nitrogen-doped titanium dioxide as visible-light-sensitive photocatalyst: designs, developments, and prospects. *Chem. Rev.* 2014, 114, 9824-52. DOI PubMed
40. Choi, W.; Termin, A.; Hoffmann, M. R. The role of metal ion dopants in quantum-sized TiO₂: correlation between photoreactivity and charge carrier recombination dynamics. *J. Phys. Chem.* 1994, 98, 13669-79. DOI
41. Li, J.; Yang, W.; Wu, A.; Zhang, X.; Xu, T.; Liu, B. Band-gap tunable 2D hexagonal (GaN)_{1-x}(ZnO)_x solid-solution nanosheets for photocatalytic water splitting. *ACS Appl. Mater. Interfaces*. 2020, 12, 8583-91. DOI
42. Tsuji, I.; Kato, H.; Kobayashi, H.; Kudo, A. Photocatalytic H₂ evolution reaction from aqueous solutions over band structure-controlled (AgIn)_xZn_{2(1-x)}S₂ solid solution photocatalysts with visible-light response and their surface nanostructures. *J. Am. Chem. Soc.* 2004, 126, 13406-13. DOI PubMed
43. Chen, J.; Chen, J.; Li, Y. Hollow ZnCdS dodecahedral cages for highly efficient visible-light-driven hydrogen generation. *J. Mater. Chem. A*. 2017, 5, 24116-25. DOI
44. Song, J.; Zhao, H.; Sun, R.; Li, X.; Sun, D. An efficient hydrogen evolution catalyst composed of palladium phosphorous sulphide (PdP_{-0.33}S_{-1.67}) and twin nanocrystal Zn_{0.5}Cd_{0.5}S solid solution with both homo- and hetero-junctions. *Energy. Environ. Sci.* 2017, 10, 225-35. DOI
45. Yu, G.; Qian, J.; Zhang, P.; et al. Collective excitation of plasmon-coupled Au-nanochain boosts photocatalytic hydrogen evolution of semiconductor. *Nat. Commun.* 2019, 10, 4912. DOI PubMed PMC
46. Zhao, H.; Li, C. F.; Yong, X.; et al. Coproduction of hydrogen and lactic acid from glucose photocatalysis on band-engineered Zn_{1-x}Cd_xS homojunction. *iScience* 2021, 24, 102109. DOI PubMed PMC
47. Liu, M.; Jing, D.; Zhou, Z.; Guo, L. Twin-induced one-dimensional homojunctions yield high quantum efficiency for solar hydrogen generation. *Nat. Commun.* 2013, 4, 2278. DOI
48. Gao, R.; Cheng, B.; Fan, J.; Yu, J.; Ho, W. Zn_xCd_{1-x}S quantum dot with enhanced photocatalytic H₂-production performance. *Chinese. J. Catal.* 2021, 42, 15-24. DOI
49. Copeland, J. R.; Santillan, I. A.; Schimming, S. M.; Ewbank, J. L.; Sievers, C. Surface interactions of glycerol with acidic and basic metal oxides. *J. Phys. Chem. C*. 2013, 117, 21413-25. DOI
50. An, Z.; Zhang, Z.; Huang, Z.; et al. Pt₁ enhanced C-H activation synergistic with Pt_n catalysis for glycerol cascade oxidation to glyceric acid. *Nat. Commun.* 2022, 13, 5467. DOI PubMed PMC
51. Sandrini, R. M.; Sempionatto, J. R.; Herrero, E.; Feliu, J. M.; Souza-Garcia, J.; Angelucci, C. A. Mechanistic aspects of glycerol electrooxidation on Pt(111) electrode in alkaline media. *Electrochem. Commun.* 2018, 86, 149-52. DOI

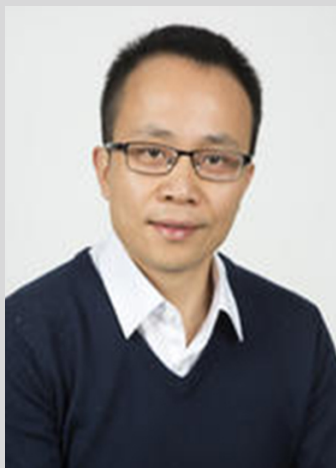


Xinti Yu

Xinti Yu completed her Master's degree in the Department of Chemical and Petroleum Engineering at the University of Calgary in 2023. She is currently a Ph.D. student at the University of Calgary under the supervision of Prof. Zhangxing Chen and Prof. Jinguang Hu. Her research centers on density functional theory (DFT) calculations related to photocatalyst design and preparation for selective biomass valorization and simultaneous H₂ production.

**Daichen Liu**

Daichen Liu completed his Master's degree in the Department of Chemical and Petroleum Engineering at the University of Calgary in 2024 under the supervision of Prof. Jinguang Hu and Prof. Keekyoung Kim. He is currently a Ph.D. student at the University of Waterloo under the supervision of Dr. Evelyn Yim. His research focuses on the improvement and in vivo study of small-diameter vascular grafts made of PVA.

**Jinguang Hu**

Jinguang Hu is an Associate Professor in the Department of Chemical and Petroleum Engineering at the University of Calgary, Canada. He received his Ph.D. from the University of British Columbia and completed his postdoctoral research at the UBC BioProducts Institute (Canada) and the Aalto-VTT HYBER Center (Academy of Finland's Centre of Excellence in Molecular Engineering of Biosynthetic Hybrid Materials research). His current research, supported by the Canada First Research Excellence Fund (CFREF), focuses on biomass valorization, sustainable energy, bioinspired materials/systems, and protein engineering for Energy, Environmental and Biomedical applications. He is a member of the External Advisory Board of the Canada Biomass Energy Network, a member of the "China-Canada Joint Centre for BioEnergy", a Research Fellow of GBIC, a recipient of "the S.C. Trindade Award", and an active participant in the International Energy Agency (IEA) Bioenergy division.

**Heng Zhao**

Heng Zhao is an Assistant Professor at the Eastern Institute of Technology in Ningbo, China. He graduated from Wuhan University of Technology in 2019 under the supervision of Academician Bao-Lian Su. He worked as Postdoctoral Associate at the University of Calgary where Academician Zhangxing Chen was his supervisor. He has published more than 80 SCI papers in top journals related to energy and environment. His research interests include but are not limited to hydrogen production, one-carbon conversion, and biomass valorization. He is a Young Innovative Talent of the Yongjiang Talent Project and youth editorial board members of *Chemical Synthesis* and *Green Carbon*.



Zhangxing Chen

Zhangxing Chen holds the rare distinction of simultaneously occupying three research chairs: Alberta Innovates (formerly iCORE) Industrial Chair in Reservoir Modeling and NSERC/Energi Simulation (formerly Foundation CMG) Senior Industrial Research Chair in Reservoir Simulation, University of Calgary, Canada and a Research Chair at Eastern Institute of Technology, Ningbo, China. He is an international leader in petroleum engineering and has made exceptional contributions to the mathematical modeling and numerical simulation of fluid flows and their applications in various industries.

Dr. Chen's outstanding contributions to engineering research, practice, and education have been recognized with numerous highest professional distinctions, including Member of National Academy of Engineering, USA, Fellow of the Royal Society of Canada, Canadian Academy of Engineering and Engineering Institute of Canada, and Academician of Chinese Academy of Engineering. He has also received numerous prestigious awards, such as the Friendship Medal of The People's Republic of China, SPE's Technical Excellence and Achievements Award, NSERC's (Natural Sciences and Engineering Research Council of Canada) Synergy Award for Innovation, Fields-CAIMS (Canadian Applied and Industrial Mathematics Society) Prize, Killam Professorship Award, IBM Faculty Award, Imperial Oil Research Award, Alberta Science and Technology Outstanding Leader Award, and Gerald J. Ford Research Award.

Dr. Chen has authored/co-authored 25 books, published over 1,200 research articles, and holds 46 patents. His publications have received 31,000 citations and an *H*-index of 72 (Google Scholar). According to Elsevier Scopus, his publications have been ranked #1 globally in terms of the overall scholarship (numbers of papers, citations, and *H*-index) in reservoir simulation. His research interests include Artificial Intelligence, Reservoir Engineering, Reservoir Simulation and Hydrogen Production.